

Preparation of modified $\text{SrAl}_{1.3}\text{Fe}_{10.7}\text{O}_{19}$ nanostructures and evaluation of size influence on its optical and magnetic properties

Reza Peymanfar¹ ✉, Abdollah Javidan², Elnaz Selseleh-Zakerin¹

¹Department of Chemical Engineering, Energy Institute of Higher Education, Saveh, PO Box 39177/67746, Iran

²Department of Basic Sciences, Imam Hossein University, Tehran, Iran

✉ E-mail: reza_peymanfar@alumni.iust.ac.ir

Published in Micro & Nano Letters; Received on 4th March 2020; Revised on 2nd June 2020; Accepted on 8th July 2020

Modifying the morphology of nanostructures and its influence on the features of the tailored nanoparticles (NPs) has attracted a great deal of interest. In this research, the morphological effect on magnetic properties of the bare or modified NPs was investigated. Bare NPs were fabricated by the sol–gel route and modified NPs were prepared using hydrophilic absorbent cotton (HAC) to architect morphology of the NPs. X-ray diffraction, field emission scanning electron microscopy, energy-dispersive X-ray spectroscopy, and Fourier transform infrared analyses confirmed that pure $\text{SrAl}_{1.3}\text{Fe}_{10.7}\text{O}_{19}$ NPs were synthesised based on the modified sol–gel method. Results indicated that HAC as a novel and affordable template modified the shape of the NPs. The obtained results by the diffuse reflection spectroscopy suggest that the optical performance of the NPs can be tuned by modifying the size of them. Additionally, the hysteresis loops of the vibrating sample magnetometer attested that the saturation magnetisation (M_s) of the modified NPs was elevated.

1. Introduction: Recently, the size of the nanoparticles (NPs) has been considered as the crucial factor tuning NPs characteristics. Morphological effects on the diverse features of the NPs including antibacterial [1], photocatalytic [2], photovoltaic [3], microwave absorbing [4], catalytic [5], and adsorbing [6] properties have been scrupulously dissected. It is well known that the augmenting heterojunction interfaces play a key role to tailor NPs features originated by more interactions of the grain boundaries by the reacting medium [7, 8]. Recently, the influence of the sintering time and temperature [9, 10] on the morphology and feature of the NPs were deeply investigated. Moreover, it is found that the leaching processes [11, 12] as well as capping agents [4, 7] pave the way for the tuning size. The obtained results have demonstrated that the tailoring size and shape can improve the magnetic characteristics, governed by Snoek's law [7, 13, 14]. Co-precipitation [15–17], sol–gel [18, 19], and hydrothermal [20–22] are the main methods applied to prepare magnetic NPs. The influence of the polymethylmethacrylate as a raw material on the magnetic features of the NPs as well as the microwave absorbing characteristics of the $\text{SrAl}_{1.3}\text{Fe}_{10.7}\text{O}_{19}$ /MWCNT/polyaniline nanocomposite have been reported [19, 23]. Moreover, microwave absorption of the $\text{SrAl}_{1.3}\text{Fe}_{10.7}\text{O}_{19}$ /MWCNT/silicone rubber and $\text{SrAl}_{1.3}\text{Fe}_{10.7}\text{O}_{19}$ /silicone rubber were deeply studied [24]. On the other hand, the eye-catching applications of the magnetic nanostructures including biomedicine [25], drug delivery [26], hyperthermia [27], magnetic resonance imaging [28], recyclable catalyst [29], microwave absorber, and so on have elevated their importance. In this research, the magnetic NPs were fabricated by the sol–gel method using hydrophilic absorbent cotton (HAC) as a novel and affordable dispersing agent as well as its effect on the morphological, crystal, optical, and magnetic characteristics was investigated.

2. Experimental

2.1. Chemicals: Chemical precursors including $\text{Al}(\text{NO}_3)_3 \cdot 9\text{H}_2\text{O}$, $\text{Sr}(\text{NO}_3)_2$, citric acid ($\text{C}_6\text{H}_8\text{O}_7 \cdot \text{H}_2\text{O}$), ammonia solution 25%, and $\text{Fe}(\text{NO}_3)_3 \cdot 9\text{H}_2\text{O}$ were purchased from MERCK.

2.2. Instruments: The 400 W ultrasonic homogeniser supplied from the hypersonic technology company was applied to prepare modified NPs. X-ray diffraction (XRD) patterns were obtained by a Philips PW1800 instrument operated by a Cu tube

(0.15418 nm), at 30 mA, $2\theta = 10$ –80, and 40 kV. The crystallite size of the nanostructures was revealed by Debye–Scherrer equation [13]. The optical performance was explored by Shimadzu MPC-2200. Field emission scanning electron microscopy (FE-SEM) micrographs, energy-dispersive X-ray spectroscopy (EDS) spectra, and elemental mapping images were obtained by Tescan Mira3, meanwhile some of the micrographs were supplied by Hitachi S-4160 FE-SEM. Chemical species were identified by Perkin Elmer RX1 Fourier-transform infrared spectroscopy (FTIR) using clear tablet prepared by dry KBr and 15 ton press. A IRI Kashan vibrating sample magnetometer at 25 Hz frequency and room temperature illustrated the magnetic behaviour of the prepared samples.

2.3. Preparation of the bare $\text{SrAl}_{1.3}\text{Fe}_{10.7}\text{O}_{19}$ by the sol–gel process: $\text{SrAl}_{1.3}\text{Fe}_{10.7}\text{O}_{19}$ NPs were formed by the sol–gel process. Initially, the Sr, Al, and Fe nitrate salts were dissolved in deionised water by a magnetic stirrer in stoichiometric ratios, after that, the citric acid in a molar amount of citric acid/sum of metal cations = 1 was dissolved in aforementioned solution. Subsequently, pH was raised around 8 by the alkaline solution and then the solution was become sol at 80°C, following that at 200°C for 3 h the gel was obtained and finally calcined at 400 and 1100°C for 1 h to form NPs.

2.4. Fabrication of modified $\text{SrAl}_{1.3}\text{Fe}_{10.7}\text{O}_{19}$ by the sol–gel route: To prepare the modified NPs, the aforementioned steps were repeated, meanwhile after adjusting pH, HAC was swelled in the solution and then it was treated for 1 h by ultrasound waves and heated at 80°C to become sol, then other steps were repeated to obtain the modified NPs.

3. Results and discussions

3.1. XRD patterns: Fig. 1 shows the XRD patterns of the bare and modified $\text{SrAl}_{1.3}\text{Fe}_{10.7}\text{O}_{19}$. The main diffraction peaks at $2\theta = 34.53^\circ$, 32.65° , 37.52° , 57.36° , 30.67° , 63.78° indexed to the (114), (017), (023), (0211), (110), (220) demonstrate that the $\text{SrAl}_{1.3}\text{Fe}_{10.7}\text{O}_{19}$ NPs were synthesised in accordance to JCPDS #: [98-011-2512] [23, 30]. Scherrer equation estimated that the crystallite size of the magnetic NPs and modified magnetite NPs are, respectively, 40.6 and 36.2 nm. The mentioned equation is given by $D = k\lambda/\beta\cos\theta$ where λ , k , β , D , and θ refer to the wave

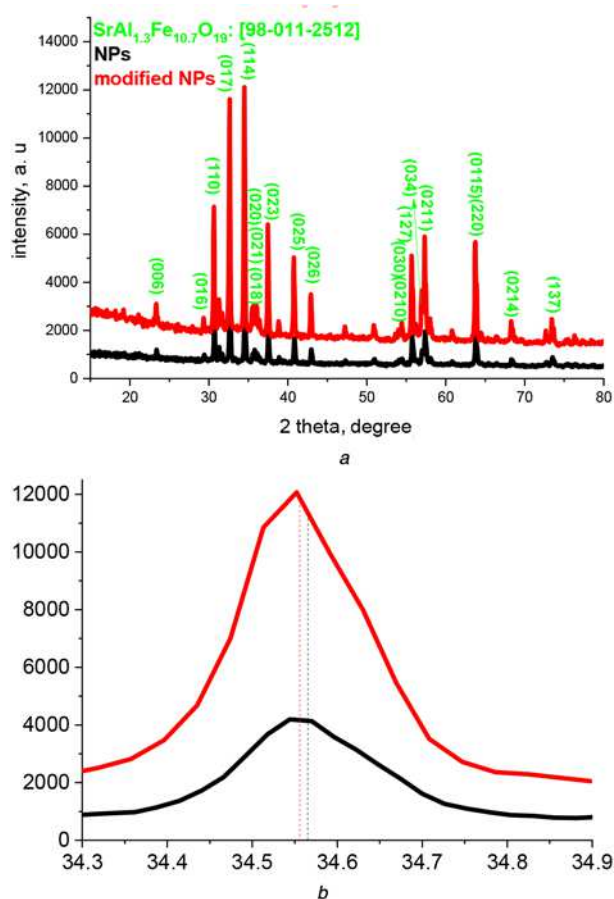


Fig. 1 XRD patterns of the bare and modified $\text{SrAl}_{1.3}\text{Fe}_{10.7}\text{O}_{19}$ NPs
a XRD patterns at $2\theta = 10\text{--}80^\circ$
b XRD patterns at $2\theta = 34.3\text{--}34.9^\circ$

length of X-ray, Scherrer constant, full width at half maximum, crystallite size, and Bragg angle, respectively [13]. The obtained results demonstrate that the size of the fabricated NPs in the presence of the organic polymer in the sol-gel method has been diminished. This could be originated by the significant distribution of the metal cations at HAC interfaces in the alkaline medium. The enhanced intensity in the modified NPs pattern indicates that using HAC promotes NPs crystallinity. It can be seen that the peak related to the (114) crystal plane was shifted from 34.565 to 34.556° attesting that d-spacing was elevated (0.001 \AA) for the modified NPs. Obviously, the organic inorganic interactions led to the reorganisation of the crystal structure of the modified NPs. Not only the electrostatic interactions between the metallic cations and unpaired electron of the hydroxyl and ether groups existing along HAC diminish agglomeration of the synthesised NPs but also the interaction of the oxygen as the electronegative atoms can regulate the crystallite size of the fabricated structures. Besides, the hydrogen bonding between the hydroxyl functional groups of the HAC and the hydroxylated intermediate modify the structure of the architected NPs [4, 7, 8, 31, 32]. The structure was formally originated from M-type hexaferrite by cationic substitution. The architected hexaferrite particles are well faceted and have the shape of hexagonal bipyramid with truncated vertexes [30].

3.2. Morphological properties and EDS spectra: FE-SEM micrographs of the $\text{SrAl}_{1.3}\text{Fe}_{10.7}\text{O}_{19}$ NPs and modified NPs are depicted in Fig. 2. The micrographs display uniform distribution of the nanostructures. The images of the modified NPs indicated that using the HAC as a dispersing agent improved the crystalline hexagonal structure. As indicated, the average size of the bare NPs is

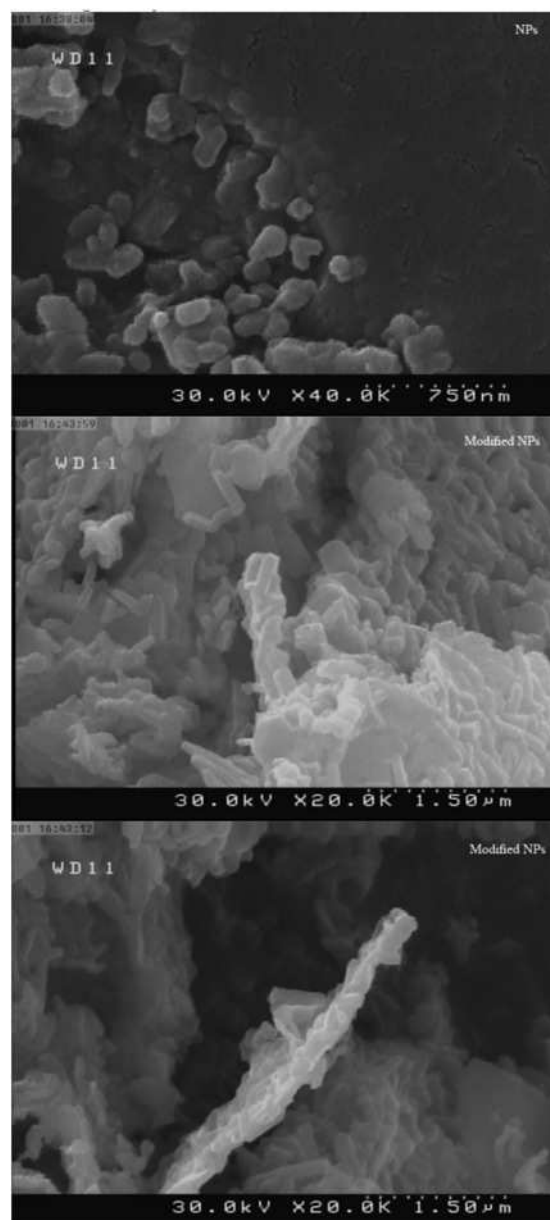


Fig. 2 FE-SEM micrographs of the $\text{SrAl}_{1.3}\text{Fe}_{10.7}\text{O}_{19}$ and modified $\text{SrAl}_{1.3}\text{Fe}_{10.7}\text{O}_{19}$ NPs

85 nm but the modified NPs showed an average size of 150 nm. Interestingly, the interfacial interactions between the cationic metals and the functional groups of the microfibrils modify the produced intermediates and then diminish the crystallite size of the tailored NPs, as given by XRD results. On the other hand, the presence of the microfibrils of HAC led to the distribution of the cationic metal on their interfaces and generating a novel hierarchical morphology of the NPs. Moreover, the occurred esterification reaction between the hydroxyl groups from HAC and the carboxyl groups from citric acid led to the novel intermediate elevating the average size of the modified NPs. It can be seen that the modified NPs have been synthesised with diminished crystallite size, meanwhile the morphology of their structure demonstrated that their average size is enhanced, realised by the produced hierarchical structure. Fig. 3 displays FE-SEM, EDS, and elemental mapping images of the samples. It can be seen the Fe, O, Al, and Sr elements exist in the fabricated structures. The elemental mapping images exhibit the uniform distributions of the atoms in the crystalline structures and attest that the carbonaceous precursors have been

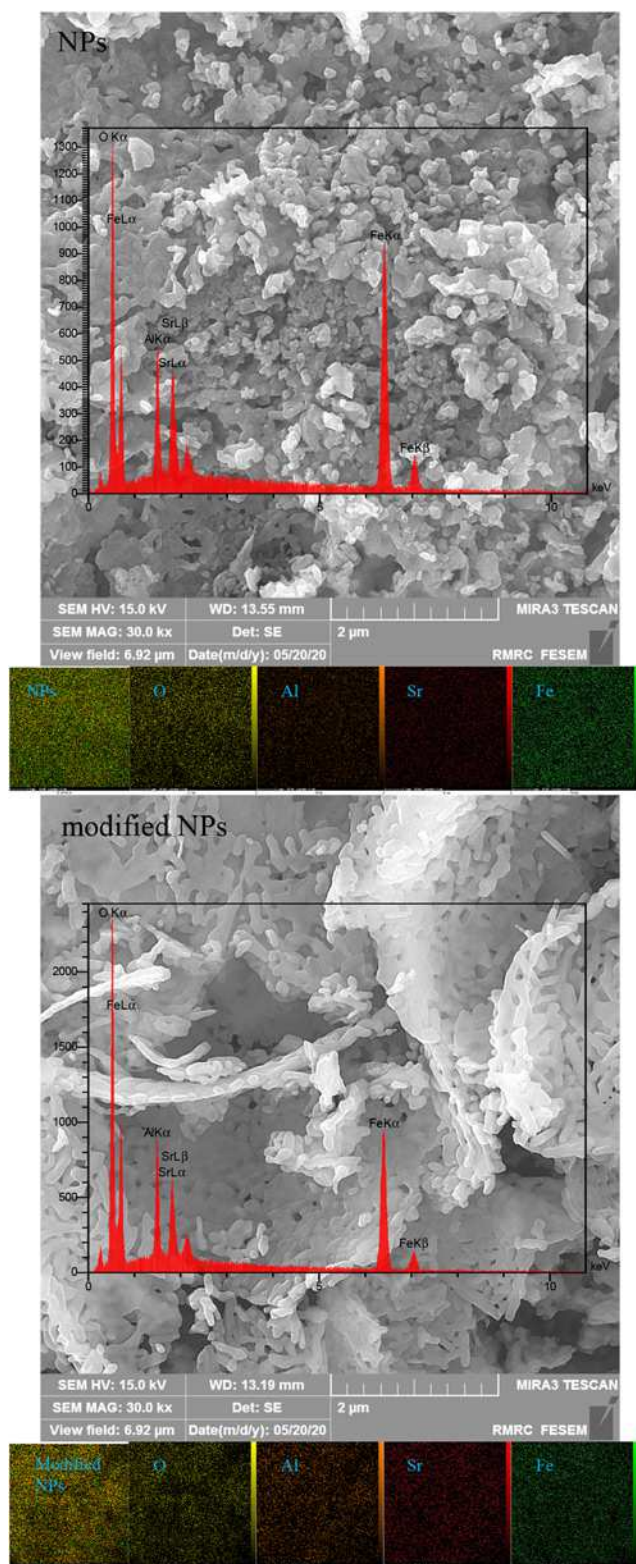


Fig. 3 FE-SEM, EDS, and elemental mapping images of the samples

eliminated. Table 1 presents a quantitative atomic (A%) and weight (W%) of the elements of structures, given by the EDS results.

3.3. FTIR spectra: The FTIR curves of the $\text{SrAl}_{1.3}\text{Fe}_{10.7}\text{O}_{19}$ and modified NPs were evaluated in Fig. 4. Three absorption peaks around 471, 627, and 792 cm^{-1} are attributed to the metal oxide stretching vibrations of the Fe–O, Al–O, and Sr–O originated from $\text{SrAl}_{1.3}\text{Fe}_{10.7}\text{O}_{19}$ and modified NPs, parallelly [23]. The

Table 1 Quantitative results of NPs and modified NPs

Elt	W%	A%	Elt	W%	A%
O	33.10	62.25	O	44.73	72.35
Al	5.39	6.01	Al	6.60	6.33
Fe	54.33	29.27	Fe	41.33	19.15
Sr	7.18	2.47	Sr	7.34	2.17
NPs	100.00	100.00	modified NPS	100.00	100.00

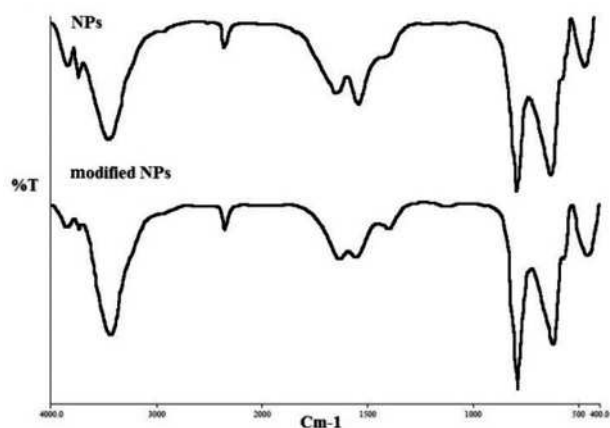


Fig. 4 FTIR spectra of the pristine and modified $\text{SrAl}_{1.3}\text{Fe}_{10.7}\text{O}_{19}$

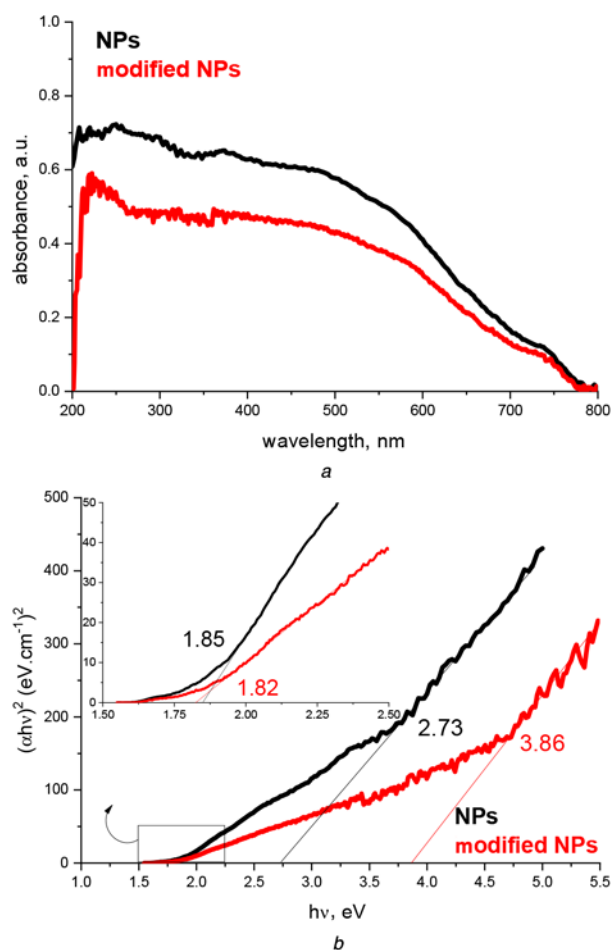


Fig. 5 Optical performance of the specimens
a UV-Vis light absorption
b Energy bandgap

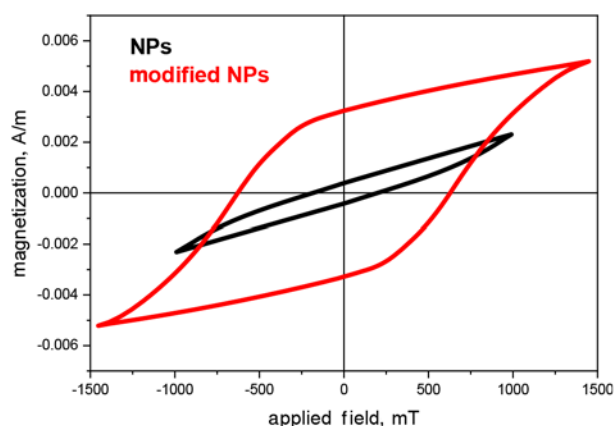


Fig. 6 M - H loops of NPs and modified NPs

Table 2 Magnetic characters of NPs and modified NPs

Entry	Sample	M_s , A/m	M_r , A/m	H_c , mT
1	NPs	0.0027	0.0004	200.5
2	modified NPs	0.0056	0.0033	625.0

shallow band at 3600 cm^{-1} and the bump at 1644 cm^{-1} are indexed to the stretching and in-plane and out-of-plane bending vibrations of O-H generated by the adsorbed water and hydroxyl functional groups existing at grain boundaries [4]. It can be seen that all of the notches ascribed to the HAC chemical structure have been eliminated after heat treatments. The observed peak at 2330 cm^{-1} is associated of the adsorbed CO_2 stretching vibration at heterojunction interfaces [7, 31].

3.4. Optical performance: Fig. 5 exposes the UV-Vis light absorptions and energy bandgaps of the specimens. The energy bandgaps were estimated based on the Kubelka-Munk theory [33–35], suggesting diverse energy bandgaps for the samples. It should be noted the energy bandgap of the modified NPs was different owing to the more over hanging bonds, supplying the more discretised energy levels for the electron jumping [31]. The more light absorption is originated from the more surface area to volume ratio of the NPs due to their smaller structure.

3.5. Magnetic features: Magnetic characters including coercivity (H_c), M_s , and remanent magnetisation (M_r) of the $\text{SrAl}_{1.3}\text{Fe}_{10.7}\text{O}_{19}$ and modified $\text{SrAl}_{1.3}\text{Fe}_{10.7}\text{O}_{19}$ NPs are evaluated by the primitive magnetisation versus applied field (M - H) loops (Fig. 6). The results are summarised in Table 2. As revealed, augmenting the crystallinity and size of the NPs using organic template elevates ferromagnetic properties of the NPs originated by more distribution of the elements in the presence of the HAC as the dispersing agent. The hydroxyl functional groups existing in the HAC led to the more distribution of the metal cations on them influencing on the crystallinity and size of the prepared NPs and their magnetic features, governed by Snoek's law [8, 14, 36, 37]. It is found that the modified NPs demonstrated the hierarchical morphology with lower surface area to volume ratio, compared to the bare NPs. The more grain boundaries boost the magnetic dead layers at interfaces diminishing the magnetic characteristics. Accordingly, the lower magnetic parameters of the bare NPs can be derived by their smaller size [4, 7, 8, 31].

4. Conclusion: In this research, the size and crystallinity effects on the magnetic properties of the $\text{SrAl}_{1.3}\text{Fe}_{10.7}\text{O}_{19}$ NPs were

investigated. The FTIR results indicated that Metal-O bonds have been formed without any excess impurity of organic precursors. The enhanced intensity of the modified NPs pattern in its XRD curve showed that the presence of HAC reduces the size of the NPs as well as boosts its crystallinity. The FE-SEM images of the modified NPs demonstrated that using HAC brings uniform hexagonal structure for the NPs. Based on the obtained results, the pure $\text{SrAl}_{1.3}\text{Fe}_{10.7}\text{O}_{19}$ NPs were synthesised by the sol-gel method. As indicated, the optical characteristic is regulated by tailoring the size of the NPs. Eventually, the hysteresis loops indicated that the enhancing crystallinity and diminishing size of the $\text{SrAl}_{1.3}\text{Fe}_{10.7}\text{O}_{19}$ nanostructures improve the ferromagnetic properties of the NPs. More significantly, the achieved results attest that the applied process can be employed to tune heterojunction interfaces and tailor their characteristics.

5 References

- [1] Mirzaei A., Peymanfar R., Khodamoradipoor N.: 'Investigation of size and medium effects on antimicrobial properties by CuCr_2O_4 nanoparticles and silicone rubber or PVDF', *Mater. Res. Express*, 2019, **6**, p. 085412
- [2] Peymanfar R., Ramezanalizadeh H.: 'Sol-gel assisted synthesis of CuCr_2O_4 nanoparticles: an efficient visible-light driven photocatalyst for the degradation of water pollutions', *Optik*, 2018, **169**, pp. 424–431
- [3] Li Z., Yu L.: 'The size effect of TiO_2 hollow microspheres on photo-voltaic performance of ZnS/Cds quantum dots sensitized solar cell', *Materials*, 2019, **12**, (10), p. 1583
- [4] Peymanfar R., Javanshir S., Naimi-Jamal M.R., *ET AL.*: 'Preparation and identification of modified $\text{La}_{0.8}\text{Sr}_{0.2}\text{FeO}_3$ nanoparticles and study of its microwave properties using silicone rubber or PVC', *Mater. Res. Express*, 2019, **6**, (7), p. 075004
- [5] Peng R., Li S., Sun X., *ET AL.*: 'Size effect of Pt nanoparticles on the catalytic oxidation of toluene over Pt/ CeO_2 catalysts', *Appl. Catal. B, Environ.*, 2018, **220**, pp. 462–470
- [6] Liu X., Sun J., Xu X., *ET AL.*: 'Adsorption and desorption of U (Vi) on different-size graphene oxide', *Chem. Eng. J.*, 2019, **360**, pp. 941–950
- [7] Peymanfar R., Azadi F.: 'Preparation and identification of bare and capped CuFe_2O_4 nanoparticles using organic template and investigation of the size, magnetism, and polarization on their microwave characteristics', *Nano-Struct. Nano-Objects*, 2019, **17**, pp. 112–122
- [8] Peymanfar R., Rahmanisaghieh M.: 'Preparation of neat and capped BaFe_2O_4 nanoparticles and investigation of morphology, magnetic, and polarization effects on its microwave and optical performance', *Mater. Res. Express*, 2018, **5**, (10), p. 105012
- [9] Moghadam A., Mirzaee O., Shokrollahi H., *ET AL.*: 'Magnetic and morphological characterization of bulk $\text{Bi}_2\text{Fe}_4\text{O}_9$ derived by reverse chemical co-precipitation: a comparative study of different sintering methods', *Ceramics Int.*, 2019, **45**, (7), pp. 8087–8094
- [10] Ramirez-Gutierrez C., Londoño-Restrepo S., Del Real A., *ET AL.*: 'Effect of the temperature and sintering time on the thermal, structural, morphological, and vibrational properties of hydroxyapatite derived from pig bone', *Ceramics Int.*, 2017, **43**, (10), pp. 7552–7559
- [11] Meija R., Signetti S., Schuchardt A., *ET AL.*: 'Nanomechanics of individual aerographite tetrapods', *Nat. Commun.*, 2017, **8**, p. 14982
- [12] Jian X., Wu B., Wei Y., *ET AL.*: 'Facile synthesis of Fe_3O_4 /Ges composites and their enhanced microwave absorption properties', *ACS Appl. Mater. Interfaces*, 2016, **8**, (9), pp. 6101–6109
- [13] Peymanfar R., Ahmadi M., Javanshir S.: 'Tailoring $\text{Go/BaFe}_{12}\text{O}_{19}/\text{La}_{0.5}\text{Sr}_{0.5}\text{MnO}_3$ ternary nanocomposite and investigation of its microwave characteristics', *Mater. Res. Express*, 2019, **6**, p. 085063
- [14] Snoek J.: 'Gyromagnetic resonance in ferrites', *Nature*, 1947, **160**, (4055), p. 90
- [15] Lu M.-M., Cao M.-S., Chen Y.-H., *ET AL.*: 'Multiscale assembly of grape-like ferromagnetic oxide and carbon nanotubes: a smart absorber prototype varying temperature to tune intensities', *ACS Appl. Mater. Interfaces*, 2015, **7**, (34), pp. 19408–19415
- [16] Bartůňek V., Huber Š., Luxa J., *ET AL.*: 'Facile synthesis of magnetic Co nanofoam by low-temperature thermal decomposition of Co glycerolate', *Micro Nano Lett.*, 2017, **12**, (5), pp. 278–280
- [17] Peymanfar R., Javanshir S., Naimi-Jamal M.R., *ET AL.*: 'Preparation and characterization of $\text{Mwnt/Zn}_{0.25}\text{Co}_{0.75}\text{Fe}_2\text{O}_4$ nanocomposite and investigation of its microwave absorption properties at X-band

- frequency using silicone rubber polymeric matrix', *J. Electron. Mater.*, 2019, **48**, (5), pp. 3086–3095
- [18] Dalal M., Greneche J.-M., Satpati B., *ET AL.*: 'Microwave absorption and the magnetic hyperthermia applications of $\text{Li}_{0.3}\text{Zn}_{0.3}\text{Co}_{0.1}\text{Fe}_{2.3}\text{O}_4$ nanoparticles in multiwalled carbon nanotube matrix', *ACS Appl. Mater. Interfaces*, 2017, **9**, (46), pp. 40831–40845
- [19] Peymanfar R., Javanshir S.: 'Preparation and characterization of $\text{Ba}_{0.2}\text{Sr}_{0.2}\text{La}_{0.6}\text{MnO}_3$ nanoparticles and investigation of size & shape effect on microwave absorption', *J. Magn. Magn. Mater.*, 2017, **432**, pp. 444–449
- [20] Moitra D., Dhole S., Ghosh B.K., *ET AL.*: 'Synthesis and microwave absorption properties of BiFeO_3 nanowire-Rgo nanocomposite and first-principles calculations for insight of electromagnetic properties and electronic structures', *J. Phys. Chem. C*, 2017, **121**, (39), pp. 21290–21304
- [21] Xu C., Wang Y., Chen H., *ET AL.*: 'Hydrothermal synthesis of chain-like nickel microstructures with enhanced magnetic properties', *Micro Nano Lett.*, 2014, **9**, (4), pp. 261–263
- [22] Han X., Xu C., Chen H.: 'Hydrothermal synthesis of novel Ni micro-flowers with enhanced ferromagnetic properties', *Micro Nano Lett.*, 2019, **14**, (4), pp. 455–457
- [23] Peymanfar R., Javidan A., Javanshir S.: 'Preparation and investigation of structural, magnetic, and microwave absorption properties of aluminum-doped strontium ferrite/mwcnt/polyaniline nanocomposite at Ku-band frequency', *J. Appl. Polym. Sci.*, 2017, **134**, (30), p. 45135
- [24] Peymanfar R., Afghahi S.S.S., Javanshir S.: 'Preparation and investigation of structural, magnetic, and microwave absorption properties of a $\text{SrAl}_{1.3}\text{Fe}_{10.7}\text{O}_{19}$ /multiwalled carbon nanotube nanocomposite in X and Ku-band frequencies', *J. Nanosci. Nanotechnol.*, 2019, **19**, (7), pp. 3911–3918
- [25] Pankhurst Q.A., Connolly J., Jones S.K., *ET AL.*: 'Applications of magnetic nanoparticles in biomedicine', *J. Phys. D: Appl. Phys.*, 2003, **36**, (13), p. R167
- [26] Arruebo M., Fernández-Pacheco R., Ibarra M.R., *ET AL.*: 'Magnetic nanoparticles for drug delivery', *Nano. Today*, 2007, **2**, (3), pp. 22–32
- [27] Thiesen B., Jordan A.: 'Clinical applications of magnetic nanoparticles for hyperthermia', *Int. J. Hyperthermia*, 2008, **24**, (6), pp. 467–474
- [28] Sun C., Lee J.S., Zhang M.: 'Magnetic nanoparticles in Mr imaging and drug delivery', *Adv. Drug Delivery Rev.*, 2008, **60**, (11), pp. 1252–1265
- [29] Yoon T.-J., Lee W., Oh Y.-S., *ET AL.*: 'Magnetic nanoparticles as a catalyst vehicle for simple and easy recycling', *New J. Chem.*, 2003, **27**, (2), pp. 227–229
- [30] Kazin P., Trusov L., Zaitsev D., *ET AL.*: 'Formation of submicron-sized $\text{SrFe}_{12}\text{-Xalxo}$ 19 with very high coercivity', *J. Magn. Magn. Mater.*, 2008, **320**, (6), pp. 1068–1072
- [31] Peymanfar R., Khodamoradipoor N.: 'Preparation and characterization of copper chromium oxide nanoparticles using modified sol-gel route and evaluation of their microwave absorption properties', *Physica Status Solidi (A)*, 2019, **216**, p. 1900057
- [32] Peymanfar R., Javanshir S.: 'Preparation and characterization of $\text{Ba}_{0.2}\text{Sr}_{0.2}\text{La}_{0.6}\text{MnO}_3$ nanoparticles and investigation of size & shape effect on microwave absorption', *J. Magn. Magn. Mater.*, 2017, **432**, pp. 444–449
- [33] Peymanfar R., Karimi J., Fallahi R.: 'Novel, promising, and broad-band microwave-absorbing nanocomposite based on the graphite-like carbon nitride/cus', *J. Appl. Polym. Sci.*, 2020, **137**, p. 48430
- [34] Peymanfar R., Azadi F.: 'La-substituted into the CuFe_2O_4 nano-structure: a study on its magnetic, crystal, morphological, optical, and microwave features', *J. Mater. Sci.-Mater. Electron.*, 2020, **31**, pp. 9586–9594
- [35] Peymanfar R., Ghorbanian-Gezaforodi S., Selseleh-Zakerin E., *ET AL.*: 'Tailoring $\text{La}_{0.8}\text{Sr}_{0.2}\text{MnO}_3/\text{La}/\text{Sr}$ nanocomposite using a novel complementary method as well as dissecting its microwave, shielding, optical, and magnetic characteristics', *Ceramics Int.*, 2020, **46**, pp. 20896–20904
- [36] Acher O., Dubourg S.: 'Generalization of Snoek's law to ferromagnetic films and composites', *Phys. Rev. B*, 2008, **77**, (10), p. 104440
- [37] Song N.-N., Yang H.-T., Liu H.-L., *ET AL.*: 'Exceeding natural resonance frequency limit of monodisperse Fe_3O_4 nanoparticles via superparamagnetic relaxation', *Sci. Rep.*, 2013, **3**, p. 3161